IEEE Access
Multidisciplinary | Rapid Review | Open Access Journal

Received August 14, 2019, accepted September 14, 2019, date of publication September 17, 2019,
date of current version September 30, 2019.

Digital Object Identifier 10.1109/ACCESS.2019.2941973

RBFN-Based Adaptive Backstepping Sliding Mode Control of an Upper-Limb Exoskeleton With Dynamic Uncertainties

QINGCONG WU, (Member, IEEE), BAI CHEN, AND HONGTAO WU
College of Mechanical and Electrical Engineering, Nanjing University of Aeronautics and Astronautics, Nanjing 210016, China

Corresponding author: Qingcong Wu (wuqc@nuaa.edu.cn)

This work was supported in part by the National Natural Science Foundation of China under Grant 51705240, in part by the Natural Science Foundation of Jiangsu Province of China under Grant BK20170783, in part by the State Key Laboratory of Robotics and System, Harbin Institute of Technology (HIT), under Grant SKLRS-2018-KF-10, and in part by the China Postdoctoral Science Foundation under Grant 2018M640480.

ABSTRACT In recent decades, robot-assisted rehabilitation therapy has been widely researched and proven to be effective in the motor function recovery of disabled individuals. In this paper, an adaptive backstepping sliding mode control approach combined with neural uncertainty observer is developed for upper-limb exoskeleton, which can help the human operator perform repetitive rehabilitation training. Firstly, a comprehensive overview about the therapeutic exoskeleton hardware and real-time control system is introduced. Then, the neural adaptive backstepping sliding mode controller (NABSMC) is developed based on radial basis function network (RBFN) to improve the trajectory tracking accuracy with external disturbances and dynamics errors. Next, the closed-loop stability of the proposed controller is demonstrated according to the Lyapunov stability theory. Finally, further experimental investigation are conducted on three volunteers to compare the control performance of NABSMC strategy with an optimal backstepping sliding mode control (OBSMC) strategy. The comparison results show that the proposed NABSMC algorithm is capable of achieving higher trajectory tracking accuracy and better step response characteristic during repetitive passive rehabilitation training.

INDEX TERMS Upper-limb exoskeleton, rehabilitation training, adaptive backstepping sliding mode control, neural uncertainty observer, Lyapunov stability theory.

I. INTRODUCTION

Loss of motor ability in upper extremity is a serious problem faced by many individuals, such as stroke patients, elderly people, and the patients with spinal cord or orthopedic injury. The statistical data from the World Health Organization show that there are over 15 million individuals surviving a stroke in the world, and 80% of the survivors may experience hemiparesis. These people present an urgent need for the expanded rehabilitation training and prolonged motion assistance in activities of daily living (ADL). According to the clinical research results of neurological rehabilitation, appropriate repetitive motion of affected extremity shows positive effects on realizing functional improvements and optimizing body balance [1]–[3]. Traditionally, the one-to-one assisted rehabilitation training manually conducted by physiotherapists has been widely applied in the clinical hemiplegia therapy. However, there are many inherent disadvantages in the manual rehabilitation training, such as high labor intensity, long time consumption, high treatment cost, poor sustainability and weak repeatability. In addition, the therapy efficacy is dependent on the personal experience and treatment skill of physiotherapist. Therefore, the application of robotic devices, known as rehabilitation robots in physiotherapy assistive areas, has captured increasing attention from around the world in recent decades. The employment of robot-based treatment has demonstrated a high capacibility to improve the motor function of affected limb of patients. Compared with the manual training, the robotic training is able to deliver high-intensity and high-efficiency training with pertinence control algorithms and, furthermore, monitor the therapy progress of patients with integrated sensing system [4]–[6].

The associate editor coordinating the review of this manuscript and approving it for publication was Jun Hu.

Currently, a vast variety of rehabilitation robots have been developed to improve the motor functions of disabled people. The existing therapeutic robots for upper limb rehabilitation training can be divided into two types based on structural characteristics, i.e., end-effector-based rehabilitation robot and exoskeleton-based rehabilitation robot [7]. The motions of end-effector system are generated from the distal segment of impaired extremity with single connection, in which no alignment between robot joints and biological joints is required. Some typical end-effector robots for upper limb training are MIME [8], GENTLE/s [9], TA-WREX [10], WFFS [11], PARM [12], DIAGNOBOT [13], CARR [14], and so on. Comparatively, exoskeleton system has a more complex structure imitating the anatomy of human skeleton and ensuring the alignment of human and robot joint axis. Some examples of upper-limb rehabilitation exoskeleton are NEUROExos [15], CAREX-7 [16], IntelliArm [17], BONES [18], RUPERT [19], RECUPERA [20], UL-EXO7 [21], and so on. The rehabilitation exoskeleton can be worn on the affected extremity of patient with multiple contacted points and, therefore, is capable of regulating the interactive forces of each joint separately.

The effectiveness of robotic rehabilitation training is directly dependent upon the control strategies applied in therapeutic devices. For the hemiplegia patients at acute phase, the patient-passive training contributes to stimulate muscle contraction and avoid motor degeneration, and it requires the affected limb passively perform repetitive reaching tasks along predefined trajectories [22]. However, due to the highly nonlinear robot dynamics, the unknown external disturbance and the movement-varying viscoelastic characteristics of biological joints, the accurate control of the rehabilitation training system shows additional complexity over the conventional manipulator. So far, different control strategies have been developed for rehabilitation robots to enhance the position control performance during repetitive reaching training. For example, a neuron proportion-integral feedforward controller with capacities of learning, adaptation, and tackling nonlinearity was proposed in [23] to reduce the position control error of a pneumatic-muscle-driven upper limb rehabilitation robot. A nonlinear sliding mode controller combined with an exponential reaching law was developed in [24], which can reduce chattering problem and deliver better tracking performance of an upper limb exoskeleton named MARSE-7. In [25], an adaptive control strategy capable of guaranteeing the safety and fault-tolerance during trajectory tracking operation was proposed for a wearable exoskeleton. In [26], a model-based fuzzy sliding mode controller with a proportional-integral-derivative sliding surface was proposed to ensure robust and optimal position control performance.

Since the exact dynamic model parameters of human-robot interaction system are difficult to obtain, many control techniques have been proposed to compensate the dynamic uncertainties. Li *et al.* [27] proposed an approximation-based iterative fuzzy backstepping controller for an exoskeleton to estimate dynamic uncertainties and compensate time-varying disturbances during forearm movement assistance. In [28], a sliding mode tracking controller with a nonlinear disturbance observer was developed for a wire-driven rehabilitation robot to deal with the unpredictable disturbances in passive training. An adaptive time-delay estimation method was developed by Brahim *et al.* [29] to estimate the unknown dynamics of an exoskeleton and perform accurate passive repetitive training. In [30], an adaptive integral terminal sliding mode controller was proposed to deal with the bounded dynamic uncertainties of exoskeleton and achieve passive rehabilitation training. In [31], an adaptive controller was developed for an exoskeleton with input saturation, and it can approximate the uncertain robotic dynamics and suppress unknown disturbances.

Neural network technology is one of the effective methods in modeling the unknown system dynamics. Until now, to the largest of our knowledge, few researches on integrating the adaptive neural-network-based approximation strategy into the backstepping sliding mode control for the rehabilitation robots have been developed. This paper is well motivated for the accurate position control of an upper limb therapeutic exoskeleton with dynamics errors and unknown disturbances. Compared with the previous works, the novel contribution of this study focuses on developing a new neural adaptive backstepping sliding mode controller (NABSMC) for an upper extremity exoskeleton, which is capable of assisting the individuals with motor disorder in accurately performing passive repetitive training. To tackle the dynamic uncertainty and guarantee the control robustness, a feedforward neural adaptive uncertainty observer is developed based on a radial basis function network (RBFN) to estimate and compensate the lumped effects of disturbances and modeling errors. The closed-loop stability of the proposed control scheme with proper parameters is demonstrated via the Lyapunov stability theorem, and the practical control performance is validated via experimental comparative research.

The rest of this paper is arranged as the following form. The overall structure of the rehabilitation exoskeleton is introduced in the Section II. The backstepping sliding mode controller, the neural adaptive uncertainty observer, and the stability analysis are presented and discussed in Section III. The experimental methods and results are provided and analyzed in Section VI. Section V draws the conclusion and future works of this paper.

II. THE UPPER-LIMB EXOSKELETON

A. MECHANICAL DESIGN

The design of the upper-limb exoskeleton for rehabilitation training is depicted in Fig. 1. The proposed exoskeleton can provide assistance to the shoulder, elbow and wrist of the right arm of wearer. There are seven actuated degrees of freedom (DOFs) to match the biological revolute joints and achieve full range of movement in ADL, i.e., shoulder internal/external rotation, shoulder abduction/adduction, shoulder flexion/extension, elbow flexion/extension, forearm

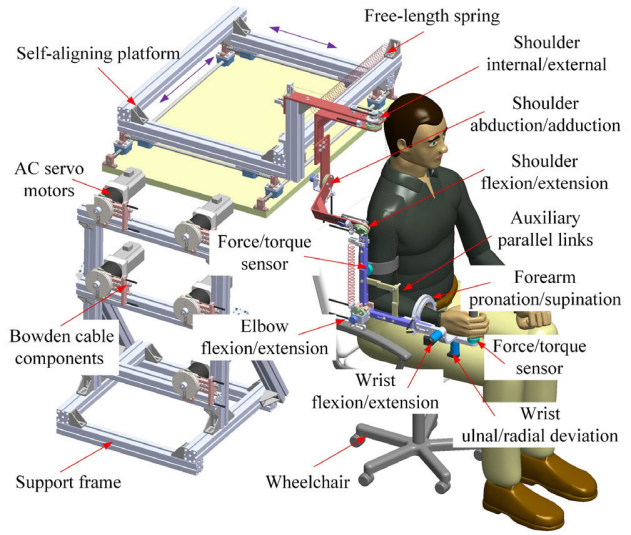

FIGURE 1. Mechanical design of the upper-limb rehabilitation exoskeleton.

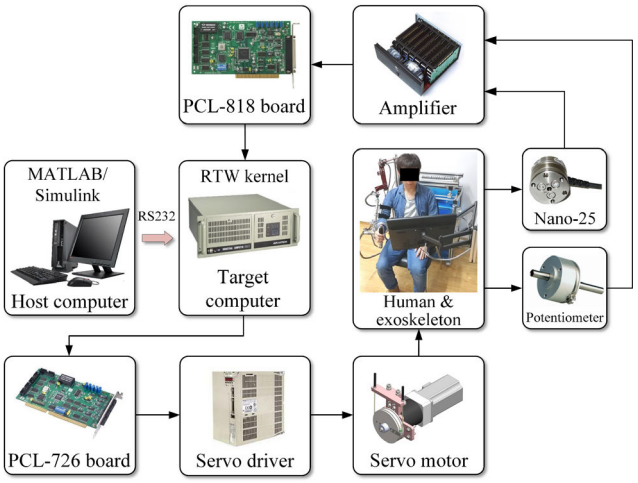

FIGURE 2. The architecture of the MATLAB/Simulink/xPC real-time control system.

pronation/supination, wrist flexion/extension and wrist ulnal/radial deviation. Besides, the exoskeleton is mounted on a self-aligning platform with two passive translational DOFs, which can compensate the misalignment of shoulder joint and improve human-robot interaction coordination. To guarantee the coincidence of robot and human joint axes, the lengths of upper arm and forearm, as well as the shoulder height, can be adjusted in accordance with the anthropometry parameters of wearer with a body height ranging from 1.6 m to 1.9 m. The actuated robot joints at shoulder and elbow are driven by the servo motors (RH-400, RENHOU) combined with flexible Bowden-cable transmission components, which are mounted on a support frame separated from exoskeleton [32]. The robotic wrist joints are driven by two coreless servo motors (JG-37, ASLONG). A passive gravity compensation mechanism, consisting of auxiliary parallel links and free-length springs, is installed in the exoskeleton to achieve the gravity-balance of the whole robotic system [33]. High-precision rotary potentiometers (WDJ22A-50K, OMTER) are encapsulated into the robot joints to measure the configuration of exoskeleton. In order to obtain the human-robot interaction forces and torques, two six-axis force/torque sensors (NANO-25, ATI) are installed on the upper arm and distal end-effector of exoskeleton. For safety consideration, mechanical end stops and dead-man buttons are integrated into the exoskeleton to avoid excessive movement and shut down the system in emergency situation.

B. ELECTRICAL CONTROL SYSTEM

Fig. 2 presents the schematic of the closed-loop real-time control system of exoskeleton, which is developed in the MATLAB/Simulink/xPC environment (2016a, Mathworks) with the real-time-workshop (RTW) core. Two industrial personal computers (IPC-610, Advantech) are utilized as the host computer and target computer of the RTW system, respectively. The host computer takes the charge of establishing Simulink control models and converting these models into corresponding executable C codes. The target computer is capable of executing the embedded target codes and controlling the movement of exoskeleton in real time. The communication between host and target layers is realized via RS232 serial port. Three industrial analog-to-digital cards (PCL-818, Advantech) are installed into the target computer to acquire the analog feedback signals from rotary potentiometers and force/torque sensors. To reduce readout noise and enhance control performance, the analog signals are filtered through a second order low-pass Butterworth filter with a cutoff frequency of 30 rad/s. In addition, two digital-to-analog cards (PCL-726, Advantech) are installed into the target computer for the purpose of converting the digital control instructions into analog output signals. The output analog signals are sent to the servo drivers to regulate the operation of servo motors. The sample frequency of the real-time control system is set to 0.1 kHz.

III. DEVELOPMENT OF NABSMC ALGORITHM

Wearable exoskeleton is a typical human-robot interaction system with highly coupling properties, as it needs to work in parallel with human limb during rehabilitation training or motion assistance. The dynamic model of the entire system, including the exoskeleton robot and biological limb, has been established in our previous research as follow [26]:

$$\tau = M(\theta)\ddot{\theta} + V(\theta,\dot{\theta})\dot{\theta} + \tau_f(\theta,\dot{\theta}) + D_u - \mathrm{J}_1^{\mathrm{T}}(\theta)\Gamma_1 - \mathrm{J}_2^{\mathrm{T}}(\theta)\Gamma_2 \tag{1}$$

Here, $\theta, \dot{\theta}$, and $\ddot{\theta} \in \mathbb{R}^7$ are the joint variable vectors of positions, velocities, and accelerations. $M(\theta) \in \mathbb{R}^{7\times7}$ is the symmetric positive-defined inertia matrix of exoskeleton. $V(\theta,\dot{\theta}) \in \mathbb{R}^7$ is the centrifugal/Coriolis matrix of exoskeleton. $\Gamma_1 \in \mathbb{R}^6$ and $\Gamma_2 \in \mathbb{R}^6$ represent the Cartesian interaction forces and torques applied on the upper arm and end-effector

of exoskeleton. $J_1(\theta) \in \mathbb{R}^{6\times7}$ and $J_2(\theta) \in \mathbb{R}^{6\times7}$ are the Jacobian matrixes that maps the human-robot interaction forces into the torques acting at robot joints. $\tau_f \in \mathbb{R}^7$ is the resultant friction from Bowden cable transmission component, motor reducers, and robot joints. $D_u \in \mathbb{R}^7$ denotes the lumped effects of dynamic uncertainties including external disturbances and modeling errors. $\tau \in \mathbb{R}^7$ represents the input vector of driving torques generating by servo motors.

Since $M(\theta)$ is symmetric positive definite, according to (1), the acceleration of exoskeleton joint can be expressed as follow:

$$\ddot{\theta} = M(\theta)^{-1}\left[\tau - V(\theta,\dot{\theta})\dot{\theta} - \tau_f(\theta,\dot{\theta}) - D_u + J_1^{\mathrm{T}}(\theta)\Gamma_1 + J_2^{\mathrm{T}}(\theta)\Gamma_2\right] \quad (2)$$

The main objective of the proposed NABSMC algorithm is to track the reference trajectory in presence of modeling error and undesirable disturbance. The position tracking error $e_1 \in \mathbb{R}^7$ and velocity tracking error $\dot{e}_1 \in \mathbb{R}^7$ are defined as follows:

$$e_1 = \theta_d - \theta \quad (3)$$

$$\dot{e}_1 = \dot{\theta}_d - \dot{\theta} \quad (4)$$

where θ_d and $\dot{\theta}_d \in \mathbb{R}^7$ represent the reference trajectory and velocity of exoskeleton joint.

The stabilizing function can be defined as follow:

$$\alpha_1 = Ce_1 \quad (5)$$

Here, $\alpha_1 \in \mathbb{R}^7$ is the stable coefficient; $C \in \mathbb{R}^{7\times7}$ represents a positive diagonal matrixes.

Then, the virtual control term $e_2 \in \mathbb{R}^7$ is defined as follow:

$$e_2 = \dot{e}_1 + \alpha_1 = \dot{\theta}_d - \dot{\theta} + \alpha_1 \quad (6)$$

Taking the derivative of e_2 with respect to t, we can have

$$\begin{aligned}\dot{e}_2 &= \ddot{\theta}_d - \ddot{\theta} + \dot{\alpha}_1 \\ &= \ddot{\theta}_d + \dot{\alpha}_1 - M(\theta)^{-1}\begin{bmatrix}\tau - V(\theta,\dot{\theta})\dot{\theta} - \tau_f(\theta,\dot{\theta}) - D_u \\ +J_1^{\mathrm{T}}(\theta)\Gamma_1 + J_2^{\mathrm{T}}(\theta)\Gamma_2\end{bmatrix}\end{aligned} \quad (7)$$

The system stability is demonstrated based on the Lyapunov stability theory [34], [35]. The first Lyapunov function candidate is chosen as

$$V_1 = \frac{1}{2}e_1^T e_1 \quad (8)$$

Differentiating V_1 with respect to time t and combining (4) and (6), we can get

$$\dot{V}_1 = e_1^T\dot{e}_1 = e_1^T(\dot{\theta}_d - \dot{\theta}) = e_1^T e_2 - e_1^T\alpha_1 = e_1^T e_2 - e_1^T Ce_1 \quad (9)$$

It can be seen that if $e_2 = 0$, $\dot{V}_1 = -e_1^T Ce_1 = -\sum_{i=1}^{7} C_i e_{1i}^2 \le 0$. Thus, it is necessary to further design the control law.

The switching function of the sliding surface $s \in \mathbb{R}^7$ is defined as follow:

$$s = \lambda e_1 + e_2 \quad (10)$$

where $\lambda \in \mathbb{R}^{7\times7}$ represents the positive diagonal matrixes of proportional gain. From (7) and (10), the deviation of the sliding variable s with respect to time t can be shown as follows:

$$\begin{aligned}\dot{s} &= \lambda\dot{e}_1 + \dot{e}_2 \\ &= \lambda\dot{e}_1 + \ddot{\theta}_d + \dot{\alpha}_1 - M(\theta)^{-1}\begin{bmatrix}\tau - V(\theta,\dot{\theta})\dot{\theta} - \tau_f(\theta,\dot{\theta}) \\ -D_u + J_1^{\mathrm{T}}(\theta)\Gamma_1 + J_2^{\mathrm{T}}(\theta)\Gamma_2\end{bmatrix} \\ &= (\lambda + C)\dot{e}_1 + \ddot{\theta}_d - M(\theta)^{-1}\begin{bmatrix}\tau - V(\theta,\dot{\theta})\dot{\theta} - \tau_f(\theta,\dot{\theta}) \\ -D_u + J_1^{\mathrm{T}}(\theta)\Gamma_1 + J_2^{\mathrm{T}}(\theta)\Gamma_2\end{bmatrix}\end{aligned} \quad (11)$$

In the design of the proposed NABSMC scheme, the control law U is composed of three terms, i.e., the equivalent control term U_{eq}, the hitting control term U_{hit}, and the disturbance compensation control term U_{dis}, and can be presented in the general form as follow:

$$U = U_{eq} + U_{hit} + U_{dis} \quad (12)$$

The equivalent control term determines the dynamic performance of control system on the sliding surface, and it can be obtained by recognizing $\dot{s} = 0$ without considering external disturbances and modeling errors. Therefore, according to (11), we can have

$$\begin{aligned}U_{eq} = M(\theta)\left[(\lambda + C)\dot{e}_1 + \ddot{\theta}_d\right] + V(\theta,\dot{\theta})\dot{\theta} + \tau_f(\theta,\dot{\theta}) \\ - J_1^{\mathrm{T}}(\theta)\Gamma_1 - J_2^{\mathrm{T}}(\theta)\Gamma_2\end{aligned} \quad (13)$$

The hitting control term, which is developed to drive the system toward the reference trajectory, is chosen as follow:

$$U_{hit} = M(\theta)\left[e_1 + Ksat(s)\right] \quad (14)$$

where $K \in \mathbb{R}^{7\times7}$ denotes a positive diagonal matrixes; $sat(s)$ denotes a saturation function with a dead-zone compensation expressed as follow:

$$sat(s_i) = \begin{cases} sign(s_i) & if\ |s_i| > \varphi \\ \dfrac{(1-\rho)s_i + \rho\varphi}{\varphi} & if\ |s_i| \le \varphi \end{cases} \quad (15)$$

Here, φ is a positive constant defining the boundary layer thickness of the saturation function; ρ represents the constant dead-zone compensation value.

The second Lyapunov function candidate is chosen as follow:

$$V_2 = V_1 + \frac{1}{2}s^T s \quad (16)$$

Differentiating V_2 with respect to time t and combining (9) and (11), we can get

$$\begin{aligned}\dot{V}_2 &= \dot{V}_1 + s^T\dot{s} \\ &= e_1^T e_2 - e_1^T Ce_1 + s^T \\ &\quad\times\left\{\begin{array}{l}(\lambda + C)\dot{e}_1 + \ddot{\theta}_d \\ -M(\theta)^{-1}\begin{bmatrix}U - V(\theta,\dot{\theta})\dot{\theta} - \tau_f(\theta,\dot{\theta}) \\ -D_u + J_1^{\mathrm{T}}(\theta)\Gamma_1 + J_2^{\mathrm{T}}(\theta)\Gamma_2\end{bmatrix}\end{array}\right\}\end{aligned} \quad (17)$$

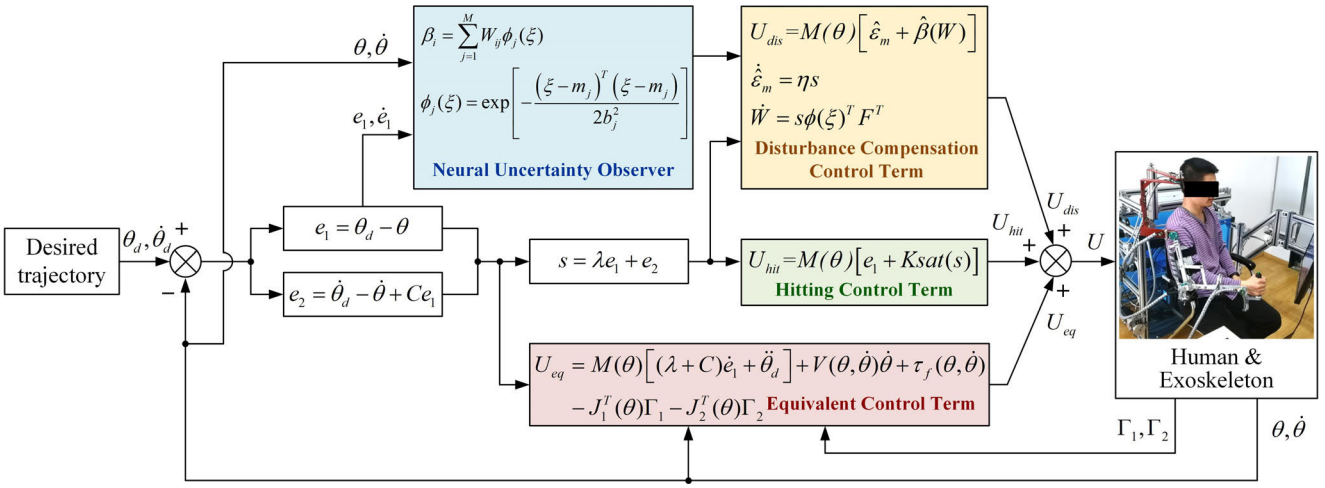

FIGURE 3. The diagram of the proposed neural adaptive backstepping sliding mode control strategy.

Inserting (13) and (14) into (17) yields

$$\begin{aligned}\dot{V}_2 &= e_1^T e_2 - e_1^T C e_1 + s^T\left[-e_1 - Ksat(s) + M(\theta)^{-1}D_u\right] \\ &= (e_2^T - s^T)e_1 - e_1^T C e_1 - s^T\left[Ksat(s) - M(\theta)^{-1}D_u\right] \\ &= -e_1^T\lambda e_1 - e_1^T C e_1 - s^T Ksat(s) + s^T M(\theta)^{-1}D_u \end{aligned} \tag{18}$$

Since the lumped uncertainty of the exoskeleton system is unknown in practical application, it is difficult to determine the boundary of the term $M(\theta)^{-1}D_u$. For simplification, we define $\beta = M(\theta)^{-1}D_u$. Then, a neural adaptive uncertainty observer is developed based on radial basis function network (RBFN) to adapt the estimated value of $\hat{\beta}$. The RBFN has been widely applied in nonlinearity approximation due to its simple architecture and fast convergence characteristic.

The structure of the three-layer RBFN, with the Gaussian function as the receptive field unit, is shown in Fig. 3. Assuming that there are M hidden nodes in the proposed RBFN, and $\phi(\xi) = [\phi_1(\xi), \phi_2(\xi), \cdots, \phi_M(\xi)]^T$ is the selected Gaussian function. The output value of the Gaussian RBFN can be calculated via the weighted sum approach defined as follows:

$$\beta_i = \sum_{j=1}^{M} W_{ij}\phi_j(\xi), \quad i = 1, 2, \cdots, N \tag{19}$$

$$\phi_j(\xi) = \exp\left[-\frac{(\xi - m_j)^T(\xi - m_j)}{2b_j^2}\right] \tag{20}$$

Here, β_i is the value of the ith output node. N denotes the number of output nodes. $\xi = \left[\theta, \dot{\theta}, e_1, \dot{e}_1\right]^T$ is the input vector of RBFN. $\phi_j(\xi)$ is the Gaussian function value for the jth neural net in the hidden layer. W_{ij} represents the weight connecting the jth hidden node to the ith output node. m_j is the center vector of the receptive field. b_j is the standard deviation of the jth neuron unit.

For the purpose of developing the adaption algorithm of the neural uncertainty observer, the minimum approximation error $\varepsilon_m \in \mathbb{R}^7$ is defined as follow:

$$\varepsilon_m = \beta - \hat{\beta}(W^*) \tag{21}$$

where W^* represents an optimal weight matrix that achieves the minimum approximation error.

Then, the disturbance compensation control term is chosen as follow:

$$U_{dis} = M(\theta)\left[\hat{\varepsilon}_m + \hat{\beta}(W)\right] \tag{22}$$

Here, $\hat{\varepsilon}_m$ represents the estimated value of the minimum approximation error.

From (12), (14) and (22), the total control law can be given as follow:

$$\begin{aligned}U = {} & M(\theta)\left[(\lambda + C)\dot{e}_1 + \ddot{\theta}_d\right] + V(\theta, \dot{\theta})\dot{\theta} + \tau_f(\theta, \dot{\theta}) - \mathrm{J}_1^{\mathrm{T}}(\theta)\Gamma_1 \\ & - \mathrm{J}_2^{\mathrm{T}}(\theta)\Gamma_2 + M(\theta)\left[e_1 + Ksat(s)\right] + M(\theta)\left[\hat{\varepsilon}_m + \hat{\beta}(W)\right] \end{aligned} \tag{23}$$

Then, the third Lyapunov function candidate is chosen as

$$V_3 = V_2 + \frac{1}{2\eta}(\varepsilon_m - \hat{\varepsilon}_m)^T(\varepsilon_m - \hat{\varepsilon}_m) + \frac{1}{2}tr(\tilde{W}F^{-1}\tilde{W}^T) \tag{24}$$

where η denotes a positive constant; F is a positive definite and diagonal matrix; $\tilde{W} = W^* - W$ represents the weight estimation error of RBFN; tr $(\cdot)$ denotes the trace operator.

Differentiating V_3 with respect to t and combining (17), (18) and (23), we can get

$$\begin{aligned}\dot{V}_3 &= \dot{V}_2 - \frac{1}{\eta}(\varepsilon_m - \hat{\varepsilon}_m)^T\dot{\hat{\varepsilon}}_m + tr(\tilde{W}F^{-1}\dot{\tilde{W}}^T) \\ &= -e_1^T\lambda e_1 - e_1^T C e_1 - s^T Ksat(s) + s^T\left[\beta - \hat{\beta}(W) - \hat{\varepsilon}_m\right] \\ &\quad - \frac{1}{\eta}(\varepsilon_m - \hat{\varepsilon}_m)^T\dot{\hat{\varepsilon}}_m + tr(\tilde{W}F^{-1}\dot{\tilde{W}}^T) \\ &= -e_1^T\lambda e_1 - e_1^T C e_1 - s^T Ksat(s) + s^T\left[\beta - \hat{\beta}(W^*) - \hat{\varepsilon}_m\right] \\ &\quad + s^T\left[\hat{\beta}(W^*) - \hat{\beta}(W)\right] - \frac{1}{\eta}(\varepsilon_m - \hat{\varepsilon}_m)^T\dot{\hat{\varepsilon}}_m \\ &\quad + tr(\tilde{W}F^{-1}\dot{\tilde{W}}^T) \end{aligned} \tag{25}$$

The adaptation laws for $\dot{\hat{\varepsilon}}_m$ and $\dot{W}$ are provided by

$$\dot{\hat{\varepsilon}}_m = \eta s \tag{26}$$

$$\dot{W} = s\phi(\xi)^T F^T \tag{27}$$

Then, inserting (21), (26) and (27) into (25), we can get

$$\begin{aligned}
\dot{V}_3 &= -e_1^T\lambda e_1 - e_1^T Ce_1 - s^T Ksat(s) + s^T(\varepsilon_m - \hat{\varepsilon}_m) \\
&\quad + s^T(W^* - W)\phi(\xi) - \frac{1}{\eta}(\varepsilon_m - \hat{\varepsilon}_m)^T\dot{\hat{\varepsilon}}_m + tr(\tilde{W}F^{-1}\dot{\tilde{W}}^T) \\
&= -e_1^T\lambda e_1 - e_1^T Ce_1 - s^T Ksat(s) + s^T(\varepsilon_m - \hat{\varepsilon}_m) \\
&\quad + s^T\tilde{W}\phi(\xi) - (\varepsilon_m - \hat{\varepsilon}_m)^T s + tr(\tilde{W}F^{-1}\dot{\tilde{W}}^T) \\
&= -e_1^T\lambda e_1 - e_1^T Ce_1 - s^T Ksat(s) + s^T\tilde{W}\phi(\xi) \\
&\quad + tr(\tilde{W}F^{-1}\dot{\tilde{W}}^T) \\
&= -e_1^T\lambda e_1 - e_1^T Ce_1 - s^T Ksat(s) \\
&\quad + tr\left[\tilde{W}\phi(\xi)s^T - \tilde{W}F^{-1}\dot{W}^T\right] \\
&= -e_1^T\lambda e_1 - e_1^T Ce_1 - s^T Ksat(s) \\
&\le -\sum_{i=1}^{7}(\lambda_{ii} + C_{ii})\,|e_{1i}| - s^T Ksat(s) \\
&\le -\sum_{i=1}^{7}\left[(\lambda_{ii} + C_{ii})\,|e_{1i}| + K_{ii}\rho\,|s_i|\right] \\
&\le 0
\end{aligned} \tag{28}$$

Here, it can be found that V_3 is positive definite while $\dot{V}_3$ is negative definite. Therefore, the proposed controller satisfies the Lyapunov stability criteria and is uniformly asymptotically stable. The position tracking error is bounded, and it gradually converges to zero and approaches the sliding surface (i.e., $s = 0$) in finite time. The external disturbances and modeling errors can be compensated via the proposed controller system. The overall block diagram of the proposed NABSMC algorithm is presented in Fig. 3.

IV. EXPERIMENTAL VERIFICATION

For the purpose of evaluating the performance and effectiveness of the developed NABSMC algorithm in passive rehabilitation training, three kinds of position tracking experiments were carried out by three healthy volunteers with different anthropometric parameters and ages (subject S1: male, height/1.72 m, weight/63 kg, age/31 years; subject S2: male, height/1.82 m, weight/72 kg, age/36 years; subject S3: female, height/1.61 m, weight/50 kg, age/26 years). The experiments include the sinusoidal trajectory tracking experiments with constant frequency and amplitude, the sinusoidal trajectory tracking experiments with time-varying frequency and amplitude, and the step response experiments with disturbance. During the experiments, the volunteers were required to comfortably sit on a wheelchair with his/her right arm equipped with exoskeleton via Velcro straps and hand grasping the end-effector. A graphical guidance screen was applied in experiments to facilitate the volunteers in understanding their real-time configuration and training condition. The scenarios of a volunteer conducting passive rehabilitation training with the proposed exoskeleton system is presented in Fig. 4. The experimental results of the developed NABSMC strategy are compared with those of the optimal backstepping sliding mode control (OBSMC) strategy [36]. The inertia matrix and the Coriolis/centrifugal matrix of dynamic model were obtained via the computer-aided virtual prototype established in the SolidWorks environment (Dassault Systems, Concord). The kinematic parameters and the dynamic parameters of the human-exoskeleton system have been introduced in detail in our previous researches [37], [38]. All participants received a detail explanation about the test procedures in advance. The ethical approval of the proposed experimental schemes has been obtained from the Institutional Review Board of the Nanjing University of Aeronautics and Astronautics.

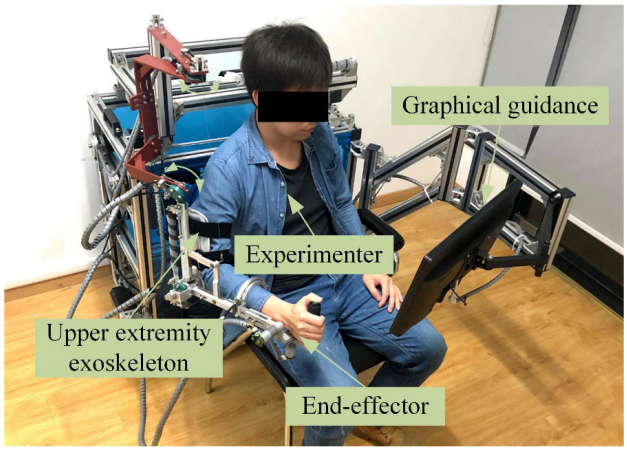

FIGURE 4. Upper-limb rehabilitation exoskeleton prototype with a healthy subject wearing the exoskeleton and performing trajectory tracking experiments.

A. TRAJECTORY TRACKING EXPERIMENTS WITH CONSTANT FREQUENCY AND AMPLITUDE

In the first experiments, the volunteers needed to perform repetitive passive training on the shoulder internal/external joint and shoulder flexion/extension joint simultaneously. The referenced trajectories of the actuated exoskeleton joints, whose servo motors were set to run in torque control mode, were defined to follow a sinusoidal trajectory with constant frequency and amplitude. Meanwhile, the other exoskeleton joints, whose servo motors were set to run in position control mode, were controlled to remain motionless during operation. The desired sinusoidal trajectory of shoulder internal/external rotation joint has a frequency of 0.5 Hz and an amplitude of 50 degrees. For the shoulder flexion/extension joint, the desired sinusoidal trajectory has a frequency of 0.5 Hz, an amplitude of 90 degrees, and a phase offset of 0.5 π. The duration of each tracking experiment was set to 10 seconds, i.e., five repetitive motion cycles.

The trajectory tracking experiments were conducted by subjects S1, S2, and S3 respectively. The results of different exoskeleton joints and control schemes are compared

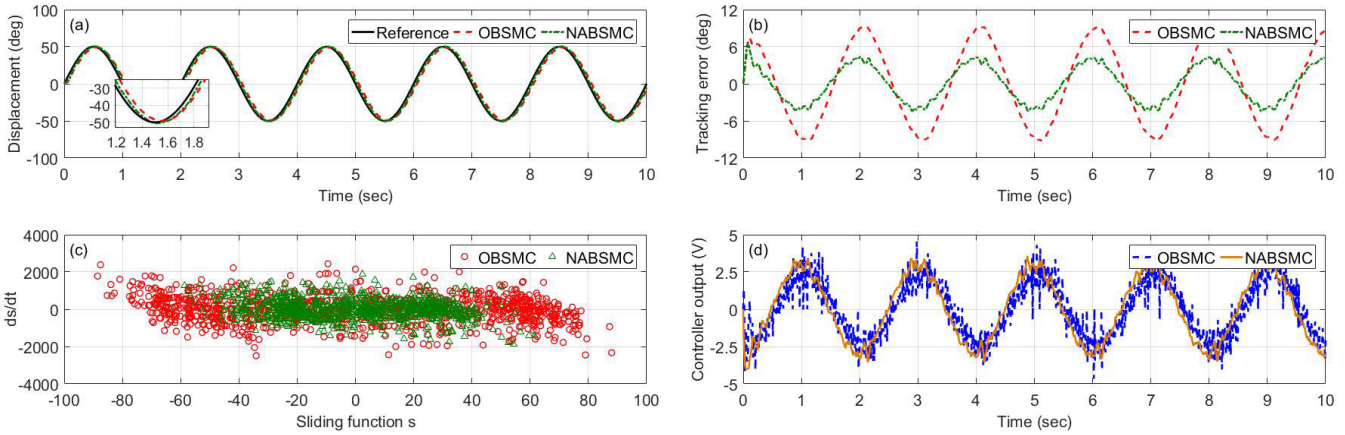

FIGURE 5. Tracking results of shoulder internal/external rotation for a sinusoidal trajectory with constant frequency and amplitude. (a) The referenced and actual trajectories of OBSMC and NABSMC. (b) Comparison of tracking errors. (c) Phase plane of s versus $\dot{s}$. (d) Control actions of OBSMC and NABSMC.

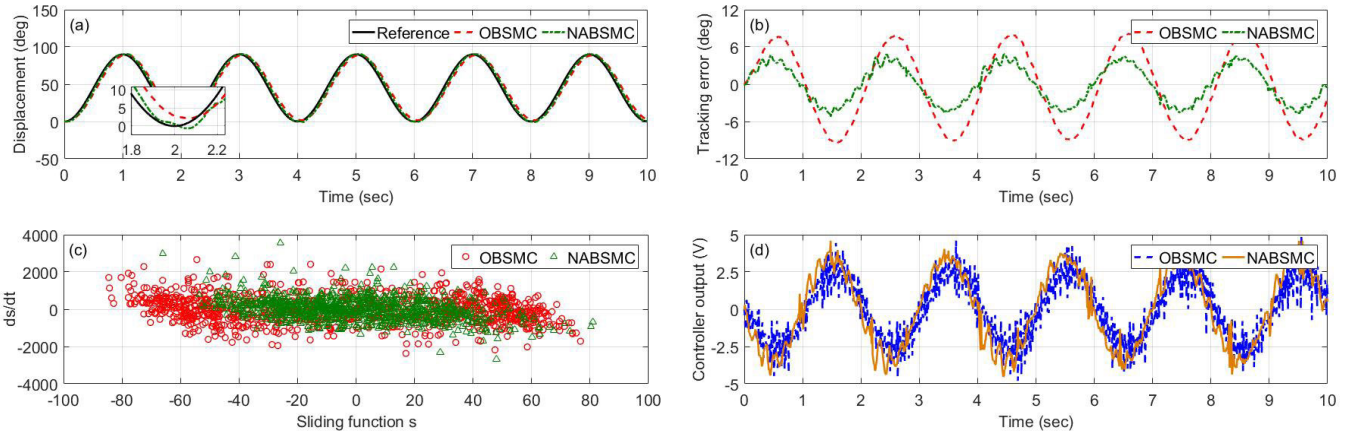

FIGURE 6. Tracking results of shoulder flexion/extension for a sinusoidal trajectory with constant frequency and amplitude. (a) The referenced and actual trajectories of OBSMC and NABSMC. (b) Comparison of tracking errors. (c) Phase plane of s versus $\dot{s}$. (d) Control actions of OBSMC and NABSMC.

and analyzed. The appropriate controller parameters of OBSMC and NABSMC were optimally tuned by the trial-and-error approach to enhance control performance and guarantee system stability. For the quantitative analysis of the control performance of different controllers, the mean absolute error (MAE), maximum absolute error (MAXE), and percentage root mean squared error (PRMSE) are defined as the following equations:

$$MAE = \frac{1}{N}\sum_{i=1}^{N}|E_i| \tag{29}$$

$$MAXE = \max|E_i| \tag{30}$$

$$PRMSE = \frac{\sqrt{\frac{1}{N}\sum_{i=1}^{N}E_i^2}}{\max(\theta_d) - \min(\theta_d)} \times 100\% \tag{31}$$

where E_i denotes the ith position tracking error data; N represents the number of data sets.

The results of the trajectory tracking experiments conducted by S1 are shown in Figs. 5 and 6. More specifically, the comparison results between the referenced trajectory and the actual trajectories are shown in Figs. 5 (a) and 6 (a). The tracking errors of OBSMC and NABSMC are presented in Figs. 5 (b) and 6 (b).

It can be clearly seen that the referenced trajectory nearly overlapped the actual ones, and the tracking errors are bounded and stable. Besides, the control performance of NABSMC, which exists smaller tracking errors, is better than that of OBSMC. For the tracking results of shoulder internal/external joint, the MAE declines from 5.56 degrees (OBSMC) to 2.57 degrees (NABSMC). Regarding the MAXE, the NABSMC algorithm gives a smaller value (i.e., 6.64 degrees) in comparison with that of OBSMC (i.e., 9.28 degrees). In addition, the PRMSE of NABSMC (i.e., 2.88%) is smaller than that of OBSMC (i.e., 6.21%). For the tracking results of shoulder flexion/extension joint, the MAE declines from 5.38 degrees (OBSMC) to 2.64 degrees (NABSMC), the MAXE declines from 9.45 degrees (OBSMC) to 5.24 degrees (NABSMC), and the PRMSE declines from 5.99% (OBSMC) to 2.96% (NABSMC), respectively. Figs. 5 (c) and 6 (c) show that the sliding

TABLE 1. Statistical results of the trajectory tracking experiments with constant frequency and amplitude.

Subject	Controller type	Shoulder internal/external rotation			Shoulder flexion/extension		
		MAE (°)	MAXE (°)	PRMSE (%)	MAE (°)	MAXE (°)	PRMSE (%)
S1	OBSMC	5.56	9.28	6.21	5.38	9.45	5.99
	NABSMC	2.57	6.64	2.88	2.64	5.24	2.96
S2	OBSMC	5.73	9.39	6.32	5.59	9.52	6.03
	NABSMC	2.98	6.81	3.06	3.01	6.33	3.25
S3	OBSMC	5.46	9.20	6.24	5.46	9.37	5.90
	NABSMC	2.51	6.72	2.75	2.79	5.88	3.10

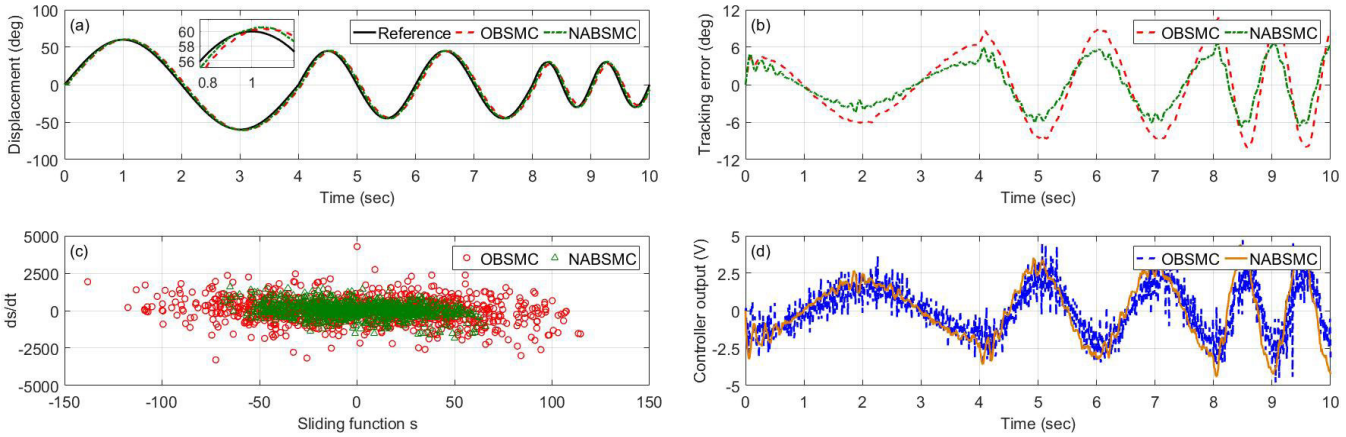

FIGURE 7. Tracking results of shoulder internal/external rotation for a sinusoidal trajectory with time-varying frequency and amplitude. (a) The referenced and actual trajectories of OBSMC and NABSMC. (b) Comparison of tracking errors. (c) Phase plane of s versus $\dot{s}$. (d) Control actions of OBSMC and NABSMC.

function s and its differential value $\dot{s}$ are well convergent in the phase plane. The controller outputs of OBSMC and NABSMC are compared in Figs. 5 (d) and 6 (d), respectively. We can observer that the chattering level of NABSMC is lower than that of OBSMC. The statistical results of the first experiments conducted by subjects S1, S2 and S3 are all tabulated in Table 1. The experimental results reveals the superiority of NABSMC over OBSMC in enhancing the trajectory tracking accuracy of passive rehabilitation training.

B. TRAJECTORY TRACKING EXPERIMENTS WITH TIME-VARYING FREQUENCY AND AMPLITUDE

In the second experiments, the volunteers were required to perform sinusoidal trajectory tracking experiments with time-varying frequency and amplitude on the shoulder internal/external and flexion/extension joints simultaneously. The duration of each tracking experiment was set to 10 seconds. The referenced sinusoidal trajectories for the shoulder internal/external rotation joint was defined to follow a frequency of 0.25 Hz and an amplitude of 60 degrees for the first four seconds, which then changed to 0.5 Hz and 45 degrees from the fourth second to the eighth second. In the last two seconds, the frequency and amplitude turned to 1 Hz and 30 degrees, respectively. On the other side, the referenced sinusoidal trajectories for the shoulder flexion/extension joint was defined to follow a frequency of 0.25 Hz and an amplitude of 100 degrees for the first four seconds, which then changed to 0.5 Hz and 80 degrees from the fourth second to the eighth second. In the last two seconds, the frequency and amplitude turned to 1 Hz and 60 degrees, respectively.

The results of the experiments under different control algorithms and conducted by different subjects are analyzed. Figs. 7 and 8 present the results of trajectory tracking experiments performed by S1. The referenced trajectory and the actual trajectories of OBSMC and NABSMC are compared in Figs. 7(a) and 8(a), while the corresponding tracking errors are shown in Figs. 7(b) and 8(b), respectively. For the tracking results of shoulder internal/external joint, the MAE declines from 4.86 degrees (OBSMC) to 3.05 degrees (NABSMC). Regarding the MAXE, the NABSMC algorithm gives a smaller value (i.e., 6.85 degrees) in comparison with that of OBSMC (i.e., 10.75 degrees). In addition, the PRMSE of NABSMC (i.e., 3.93%) is smaller than that of OBSMC (i.e., 5.58%). For the tracking results of shoulder flexion/extension joint, the MAE declines from 4.98 degrees (OBSMC) to 2.81 degrees (NABSMC), the MAXE declines from

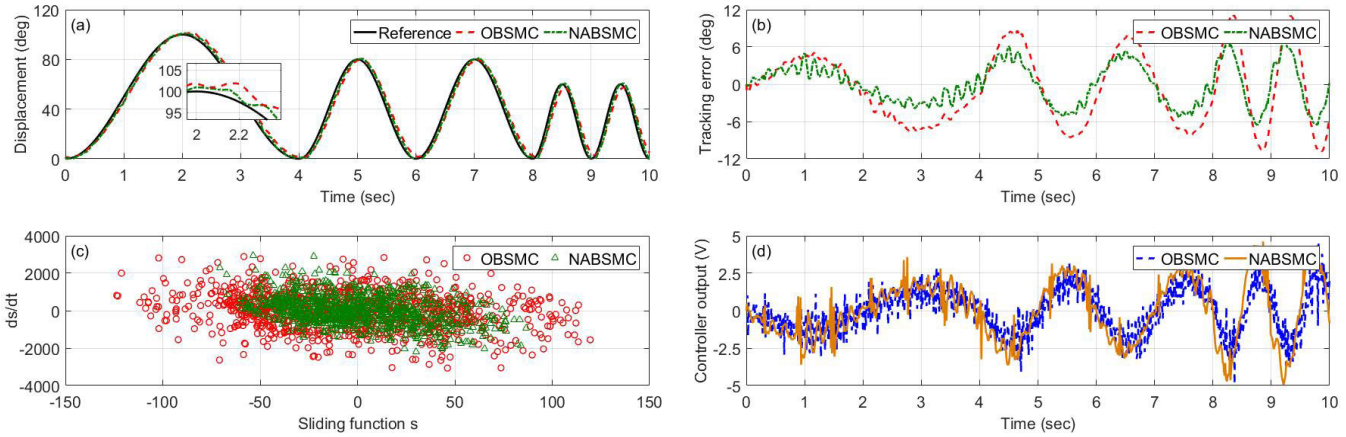

FIGURE 8. Tracking results of shoulder flexion/extension for a sinusoidal trajectory with time-varying frequency and amplitude. (a) The referenced and actual trajectories of OBSMC and NABSMC. (b) Comparison of tracking errors. (c) Phase plane of s versus $\dot{s}$. (d) Control actions of OBSMC and NABSMC.

TABLE 2. Statistical results of the trajectory tracking experiments with time-varying frequency and amplitude.

Subject	Controller type	Shoulder internal/external rotation			Shoulder flexion/extension		
		MAE (°)	MAXE (°)	PRMSE (%)	MAE (°)	MAXE (°)	PRMSE (%)
S1	OBSMC	4.86	10.75	5.58	4.98	11.30	5.77
	NABSMC	3.05	6.85	3.93	2.81	7.46	3.68
S2	OBSMC	5.01	11.12	5.70	5.11	11.04	5.65
	NABSMC	3.14	6.70	4.05	3.03	7.63	3.82
S3	OBSMC	4.93	10.95	5.63	5.05	10.99	5.70
	NABSMC	2.92	6.55	3.71	2.79	7.33	3.59

11.30 degrees (OBSMC) to 7.46 degrees (NABSMC), and the PRMSE declines from 5.77% (OBSMC) to 3.68% (NABSMC), respectively. Figs. 7 (c) and 8 (c) indicate that the sliding function s and its differential value $\dot{s}$ are well convergent in the phase plane. Furthermore, from the controller outputs of different algorithms presented in Figs. 7(d) and 8(d), it can be clearly found that the chattering level of NABSMC is lower than that of OBSMC. The statistical results of the second experiments conducted by subjects S1, S2 and S3 are all tabulated in Table 2. Therefore, it can be observed that, for the trajectory with time-varying frequency and amplitude, the position tracking control performance of NABSMC is better than that of OBSMC during rehabilitation training.

C. STEP RESPONSE EXPERIMENTS WITH EXTERNAL DISTURBANCE

In the third experiments, the volunteer needed to passively follow step response trajectory with their shoulder internal/external and flexion/extension joints separately. The duration of each tracking experiment was set to 12 seconds. The step input function was defined to rotate the shoulder to the angular position of 60 degrees at the time of 2 s. In addition, to evaluate the robustness of each control strategy with external disturbance, an impulse force with a value about 20 N was applied to the end-effector at the time around 10 s. The direction of impulse force was set to be opposite to the direction of step action. The value of impulse force was measured via the force/torque sensor.

The step response experiments were performed by subjects S1, S2 and S3 respectively. The results of the step response experiments conducted by S1 are shown in Figs. 9 and 10. More specifically, the referenced trajectory and the actual trajectories of OBSMC and NABSMC are compared in Figs. 9(a) and 10(a), while the corresponding tracking errors are shown in Figs. 9(b) and 10(b). The relation between sliding function s and its differential value $\dot{s}$ are presented in Figs. 9(c) and 10 (c). The measured impulse force are shown in Figs. 9 (d) and 10 (d). For the purpose of quantitatively evaluating the performance of step response experiments under different controllers, the rise time (RT), the setting time (ST), the overshoot of step response (OSR), the overshoot caused by disturbance (OSD), and the duration of disturbance transient phase (DTP) are calculated for the analysis and comparison of experimental results.

For the step response results of shoulder internal/external joint, the RT of NABSMC (i.e., 0.29 s) is smaller than that of the OBSMC (i.e., 0.39 s). Regarding the ST, the NABSMC algorithm gives a smaller value (i.e., 0.39 s) in comparison with that of OBSMC (i.e., 1.42 s). In addition, the OSR of NABSMC (i.e., 7.33%) is also smaller than that of OBSMC

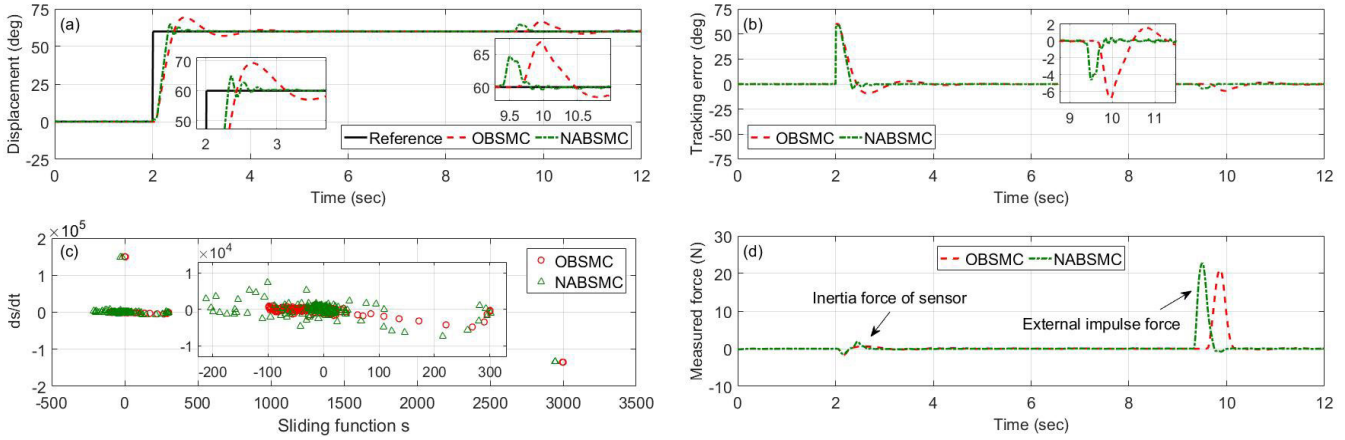

FIGURE 9. Tracking results of shoulder internal/external rotation joint for a step response trajectory with external disturbance. (a) The referenced and actual trajectories of OBSMC and NABSMC. (b) Comparison of tracking errors. (c) Phase plane of s versus $\dot{s}$. (d) Measured forces of OBSMC and NABSMC.

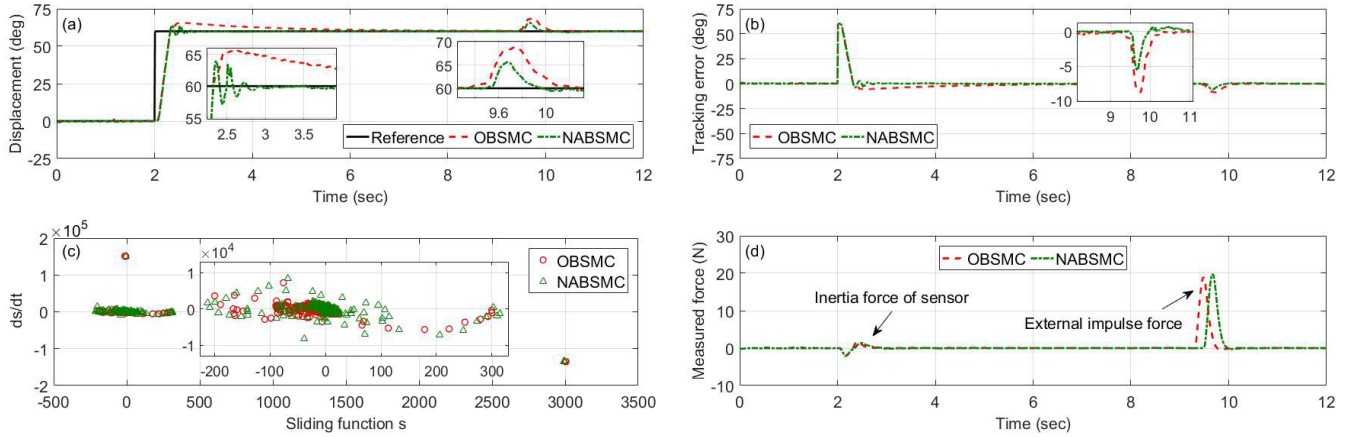

FIGURE 10. Tracking results of shoulder flexion/extension rotation joint for a step response trajectory with external disturbance. (a) The referenced and actual trajectories of OBSMC and NABSMC. (b) Comparison of tracking errors. (c) Phase plane of s versus $\dot{s}$. (d) Measured forces of OBSMC and NABSMC.

TABLE 3. Statistical results of the step response experiments with external disturbance.

Subject	Controller type	Shoulder internal/external rotation joint					Shoulder flexion/extension rotation joint				
		RT (s)	ST (s)	OSR (%)	OSD (%)	DTP (s)	RT (s)	ST (s)	OSR (%)	OSD (%)	DTP (s)
S1	OBSMC	0.39	1.42	15.1	11.4	1.39	0.30	1.35	9.26	14.7	0.86
	NABSMC	0.29	0.39	7.33	6.65	0.46	0.30	0.46	6.42	8.30	0.40
S2	OBSMC	0.43	1.37	16.2	13.5	1.23	0.35	1.22	10.7	12.4	1.15
	NABSMC	0.32	0.43	6.95	7.30	0.42	0.31	0.45	6.18	7.67	0.51
S3	OBSMC	0.46	1.28	14.9	12.7	0.98	0.32	1.41	13.1	14.5	0.97
	NABSMC	0.30	0.36	7.58	5.99	0.53	0.32	0.50	7.09	7.12	0.44

(i.e., 15.1%). The OSD (i.e., 6.65%) and DTP (i.e., 0.46 s) of NABSMC obtain smaller values in comparison with the OSD (i.e., 11.4%) and DTP (i.e., 1.39 s) of OBSMC. The results of shoulder flexion/extension joint experiment are similar to those of shoulder internal/external joint. The RT of NABSMC (i.e., 0.30 s) is equal to that of the OBSMC. Meanwhile, the ST (i.e., 0.46 s) and OSR (i.e., 6.42%) of NABSMC obtain smaller values in comparison with the ST (i.e., 1.35 s) and OSR (i.e., 9.26%) of OBSMC. In addition, the OSD (i.e., 8.30%) and DTP (i.e., 0.40 s) of NABSMC are also smaller than those of OBSMC (OSD: 14.7%, DTP: 0.86 s). The statistical results of the first experiments conducted by subjects S1, S2 and S3 are all tabulated in Table 3. Therefore, it can be concluded from the experimental results that the step

response characteristics of NABSMC algorithm are better than those of the OBSMC algorithm. Moreover, the proposed RBFN-based uncertainty observer can reduce the effect of external disturbance and improve control robustness during passive training.

V. CONCLUSION

In this paper, a novel neural adaptive backstepping sliding mode control strategy has been developed for the upper-limb exoskeleton performing rehabilitation training tasks. The lumped nonlinear uncertainty and external disturbance of the human-robot interaction system are estimated via a neural adaptive observer. By employing the Lyapunov stability theorem, the stability and boundedness of the proposed closed-loop system are proved. With the aim of validating the effectiveness of the proposed control algorithm, three typical trajectory tracking experiments were conducted on three volunteers wearing the exoskeleton. The control performance of NABSMC algorithm is compared with that of OBSMC algorithm. The experimental results indicate that the proposed NABSMC algorithm can achieve higher position control accuracy, better step response property, and higher robustness during repetitive passive training.

Future works will be devoted to integrating the recognition strategy of patient's motion intention into the control scheme and realizing the cooperative rehabilitation training suitable for the patients at the recovery period of hemiplegia. Besides, a visualization evaluation system will be proposed to monitor the therapy progress of patients and optimize control strategy.

REFERENCES

[1] L. Cheng, M. Chen, and Z. Li, "Design and control of a wearable hand rehabilitation robot," *IEEE Access*, vol. 6, pp. 74039–74050, 2018.

[2] S. Qiu, Z. Wang, H. Zhao, L. Liu, and Y. Jiang, "Using body-worn sensors for preliminary rehabilitation assessment in stroke victims with gait impairment," *IEEE Access*, vol. 6, pp. 31249–31258, 2018.

[3] Y. Zou, N. Wang, H. Ma, K. Liu, and X. Wang, "Design and experimental research of movable cable-driven lower limb rehabilitation robot," *IEEE Access*, vol. 7, pp. 2315–2326, 2018.

[4] B. Chen, C.-H. Zhong, X. Zhao, H. Ma, L. Qin, and W.-H. Liao, "Reference joint trajectories generation of CUHK-EXO exoskeleton for system balance in walking assistance," *IEEE Access*, vol. 7, pp. 33809–33821, 2019.

[5] Q. Wu, X. Wang, B. Chen, and H. Wu, "Development of a minimal-intervention-based admittance control strategy for upper extremity rehabilitation exoskeleton," *IEEE Trans. Syst., Man, Cybern., Syst.*, vol. 48, no. 6, pp. 1005–1016, Jun. 2018.

[6] Q. Wu, X. Wang, B. Chen, and H. T. Wu, "Design and fuzzy sliding mode admittance control of a soft wearable exoskeleton for elbow rehabilitation," *IEEE Access*, vol. 6, pp. 60249–60263, 2018.

[7] F. Molteni, G. Gasperini, E. Guanziroli, and G. Cannaviello, "Exoskeleton and end-effector robots for upper and lower limbs rehabilitation: Narrative review," *PM R*, vol. 10, no. 9, pp. s174–s188, 2018.

[8] C. G. Burgar, P. S. Lum, S. L. Garber, H. F. Van der Loos, D. Kenney, P. Shor, and A. M. Scremin, "Robot-assisted upper-limb therapy in acute rehabilitation setting following stroke: Department of veterans affairs multisite clinical trial," *J. Rehabil. Res. Dev.*, vol. 48, no. 4, pp. 445–458, 2011.

[9] L. Rui, F. Amirabdollahian, B. Driessen, W. Harwin, and M. Topping, "Upper limb robot mediated stroke therapy–GENTLE/s approach," *Auton. Robots.*, vol. 15, pp. 35–51, Jul. 2003.

[10] C. L. Jones and D. G. Kamper, "Involuntary neuromuscular coupling between the thumb and finger of stroke survivors during dynamic movement," *Frontiers Neurol.*, vol. 9, no. 84, pp. 1–11, 2018.

[11] L. C. Miller, R. Ruiz-Torres, A. H. A. Stienen, and J. P. A. Dewald, "A wrist and finger force sensor module for use during movements of the upper limb in chronic hemiparetic stroke," *IEEE Trans. Biomed. Eng.*, vol. 56, no. 9, pp. 2312–2317, Sep. 2009.

[12] H. Guang, L. Ji, Y. Shi, and B. J. E. Misgeld, "Dynamic modeling and interactive performance of PARM: A parallel upper-limb rehabilitation robot using impedance control for patients after stroke," *J. Healthcare Eng.*, vol. 2018, Apr. 2018, Art. no. 8647591.

[13] M. E. Aktan and E. Akdoğan, "Design and control of a diagnosis and treatment aimed robotic platform for wrist and forearm rehabilitation: DIAGNOBOT," *Adv. Mech. Eng.*, vol. 10, no. 1, pp. 1–10, 2018.

[14] M. Zhang, S. Q. Xie, X. Li, G. Zhu, W. Meng, X. Huang, and A. J. Veale, "Adaptive patient-cooperative control of a compliant ankle rehabilitation robot (CARR) with enhanced training safety," *IEEE Trans. Ind. Electron.*, vol. 65, no. 2, pp. 1398–1407, Feb. 2018.

[15] T. Lenzi, S. M. M. D. Rossi, N. Vitiello, and M. C. Carrozza, "Intention-based EMG control for powered exoskeletons," *IEEE Trans. Biomed. Eng.*, vol. 59, no. 8, pp. 2180–2190, Aug. 2012.

[16] X. Cui, W. Chen, X. Jin, and S. K. Agrawal, "Design of a 7-DOF cable-driven arm exoskeleton (CAREX-7) and a controller for dexterous motion training or assistance," *IEEE/ASME Trans. Mechatronics*, vol. 22, no. 1, pp. 161–172, Feb. 2016.

[17] Y. Ren, S. H. Kang, H. S. Park, Y. N. Wu, and L. Q. Zhang, "Developing a multi-joint upper limb exoskeleton robot for diagnosis, therapy, and outcome evaluation in neurorehabilitation," *IEEE Trans. Neural Syst. Rehabil. Eng.*, vol. 21, no. 3, pp. 490–499, May 2013.

[18] J. Klein, S. Spencer, J. E. Bobrow, D. J. Reinkensmeyer, and J. Allington, "Optimization of a parallel shoulder mechanism to achieve a high-force, low-mass, robotic-arm exoskeleton," *IEEE Trans Robot.*, vol. 26, no. 4, pp. 710–715, Aug. 2010.

[19] J. Huang, X. Tu, and J. He, "Design and evaluation of the RUPERT wearable upper extremity exoskeleton robot for clinical and in-home therapies," *IEEE Trans. Syst., Man, Cybern., Syst.*, vol. 46, no. 7, pp. 926–935, Jul. 2016.

[20] S. Kumar, H. Wöhrle, M. Trampler, M. Simnofske, H. Peters, M. Mallwitz, E. A. Kirchner, and F. Kirchner, "Modular design and decentralized control of the recupera exoskeleton for stroke rehabilitation," *Appl. Sci.*, vol. 9, no. 4, p. 626, 2019.

[21] H. Kim, L. M. Miller, I. Fedulow, M. Simkins, G. M. Abrams, N. Byl, and J. Rosen, "Kinematic data analysis for post-stroke patients following bilateral versus unilateral rehabilitation with an upper limb wearable robotic system," *IEEE Trans. Neural Syst. Rehabil. Eng.*, vol. 21, no. 2, pp. 153–164, Mar. 2013.

[22] M. H. Rahman, M. Saad, P. S. Archambault, and J. P. Kenné, "Nonlinear sliding mode control implementation of an upper limb exoskeleton robot to provide passive rehabilitation therapy," in *Intelligent Robotics and Applications* (Lecture Notes in Computer Science), vol. 7507. Berlin, Germany: Springer, 2012, pp. 52–62.

[23] X.-Z. Jiang, X.-H. Huang, R.-L. Sun, Y.-L. Xiong, and C.-H. Xiong, "Position control of a rehabilitation robotic joint based on neuron proportion-integral and feedforward control," *J. Comput. Nonlinear Dyn.*, vol. 7, no. 2, 2012, Art. no. 024502.

[24] M. H. Rahman, M. Saad, J.-P. Kenné, and P. S. Archambault, "Control of an exoskeleton robot arm with sliding mode exponential reaching law," *Int. J. Control, Autom. Syst.*, vol. 11, no. 1, pp. 92–104, 2013.

[25] H.-B. Kang and J.-H. Wang, "Adaptive control of 5 DOF upper-limb exoskeleton robot with improved safety," *ISA Trans.*, vol. 52, no. 6, pp. 844–852, 2013.

[26] Q. Wu, X. Wang, R. Xi, and F. Du, "Modeling and position control of a therapeutic exoskeleton targeting upper extremity rehabilitation," *Proc. Inst. Mech. Eng. C, J. Mech. Eng. Sci.*, vol. 231, no. 23, pp. 4360–4373, 2017.

[27] Z. Li, C.-Y. Su, G. Li, and H. Su, "Fuzzy approximation-based adaptive backstepping control of an exoskeleton for human upper limbs," *IEEE Trans. Fuzzy Syst.*, vol. 23, no. 3, pp. 555–566, Jun. 2015.

[28] J. Niu, Q. Yang, R. Song, and X. Wang, "Sliding mode tracking control of a wire-driven upper-limb rehabilitation robot with nonlinear disturbance observer," *Frontiers Neurol.*, vol. 8, p. 646, Dec. 2017.

[29] B. Brahmi, M. Saad, C. Ochoa-Luna, M. H. Rahman, and A. Brahmi, "Adaptive tracking control of an exoskeleton robot with uncertain dynamics based on estimated time-delay control," *IEEE/ASME Trans. Mechatronics*, vol. 23, no. 2, pp. 575–585, Apr. 2018.

[30] A. Riani, T. Madani, A. Benallegue, and K. Djouani, "Adaptive integral terminal sliding mode control for upper-limb rehabilitation exoskeleton," *Control Eng. Pract.*, vol. 75, pp. 108–117, Jun. 2018.
[31] W. He, Z. Li, Y. Dong, and T. Zhao, "Design and adaptive control for an upper limb robotic exoskeleton in presence of input saturation," *IEEE Trans. Neural Netw. Learn. Syst.*, vol. 30, no. 1, pp. 97–108, Jan. 2019.
[32] Q. Wu, X. Wang, L. Chen, and F. Du, "Transmission model and compensation control of double-tendon-sheath actuation system," *IEEE Trans. Ind. Electron.*, vol. 62, no. 3, pp. 1599–1609, Mar. 2015.
[33] Q. Wu, X. Wang, and F. Du, "Development and analysis of a gravity-balanced exoskeleton for active rehabilitation training of upper limb," *Proc. Inst. Mech. Eng. C, J. Mech. Eng. Sci.*, vol. 230, no. 20, pp. 3777–3790, 2016.
[34] Q. Wu, X. Wang, H. Wu, and B. Chen, "Patient-active control of a powered exoskeleton targeting upper limb rehabilitation training," *Frontiers Neurol.*, vol. 8, p. 817, Oct. 2018.
[35] C. Liu, X. Mao, X. Xu, and H. Zhang, "Stability analysis of discrete-time switched T-S fuzzy systems with all subsystems unstable," *IEEE Access*, vol. 7, pp. 50412–50418, 2019.
[36] M. Vijay and D. Jena, "Optimal backstepping sliding mode control for robot manipulator," in *Proc. IEEE Int. Conf. Signal Process., Inform., Commun. Energy*, Feb. 2015, pp. 1–5.
[37] Q.-C. Wu, X.-S. Wang, and F.-P. Du, "Analytical inverse kinematic resolution of a redundant exoskeleton for upper-limb rehabilitation," *Int. J. Hum. Robot.*, vol. 13, no. 3, 2016, Art. no. 1550042.
[38] Q. C. Wu and H. T. Wu, "Development, dynamic modeling, and multimodal control of a therapeutic exoskeleton for upper limb rehabilitation training," *Sensors*, vol. 18, no. 11, p. 3611, 2018.

QINGCONG WU received the B.S. and Ph.D. degrees in mechatronics engineering from Southeast University, Nanjing, China, in 2011 and 2016, respectively. He is currently an Assistant Professor with the College of Mechanical and Electrical Engineering, Nanjing University of Aeronautics and Astronautics, Nanjing, China. His research interests include robotics, human–robot interaction control, tendon-sheath transmission theory, gravity balancing theory, and the application of exoskeleton to neuromuscular rehabilitation.

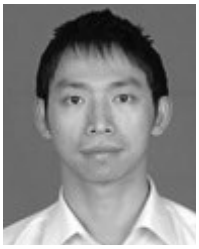

BAI CHEN received the B.S. and Ph.D. degrees in mechanical engineering from Zhejiang University, Hangzhou, China, in 2000 and 2005, respectively. He is currently a Full Professor with the College of Mechanical and Electrical Engineering, Nanjing University of Aeronautics and Astronautics. His current research interests include minimally invasive neurosurgery robot, virtual surgery systems, force feedback control, and interventional therapy.

HONGTAO WU received the B.S. degree from Yanshan University, Hebei, China, in 1982, and the M.S. and Ph.D. degrees from Tianjin University, Tianjin, China, in 1985 and 1992, respectively, all in mechanical engineering. He is currently a Full Professor with the College of Mechanical and Electrical Engineering, Nanjing University of Aeronautics and Astronautics. His current research interests include parallel robot, robot kinematics, and multibody system dynamics.